Original Article

Radiosynthesis and evaluation of an ¹⁸F-labeled radioligand for imaging metabotropic glutamate receptor 3 with positron emission tomography

Jian Rong¹, Chunyu Zhao¹, Ahmad F Chaudhary¹, Jiahui Chen¹, Yinlong Li¹, Xin Zhou¹, Zhendong Song¹, Zhenkun Sun², Yabiao Gao¹, Siyan Feng¹, Taoqian Zhao¹, Qi-Long Hu¹, Chongjiao Li¹, Achi Haider¹, Jimmy Patel^{1,3}, Chongzhao Ran⁴, Hongjie Yuan², Steven H Liang¹

¹Department of Radiology and Imaging Sciences, Emory University, Atlanta, Georgia 30322, The United States; ²Department of Pharmacology and Chemical Biology, Emory University School of Medicine, Atlanta, Georgia 30322, The United States; ³Department of Radiation Oncology, Winship Cancer Institute of Emory University, Atlanta, Georgia 30322, The United States; ⁴Athinoula A. Martinos Center for Biomedical Imaging, Department of Radiology, Massachusetts General Hospital and Harvard Medical School, Boston, Massachusetts 02114, The United States

Received May 23, 2025; Accepted September 26, 2025; Epub October 25, 2025; Published October 30, 2025

Abstract: The metabotropic glutamate receptor 3 (mGluR3) is a G-protein-coupled receptor (GPCR) involved in modulating glutamatergic neurotransmission and maintaining neural homeostasis. By inhibiting adenylyl cyclase activity, mGluR3 negatively modulates the activity of adenylyl cyclase via Gi/o protein coupling, reducing cyclic AMP (cAMP) levels and modulating downstream signaling pathways. Dysfunction of mGluR3 is associated with a range of neurological and psychiatric disorders, including depression, autism, cognitive impairment, bipolar affective disorder, schizophrenia, and neurodegenerative diseases. Despite its therapeutic relevance, no selective mGluR3 positron emission tomography (PET) radioligand is currently available to image this target *in vivo*. In this study, we report the radiosynthesis and preclinical evaluation of [18 F]VU6010572 - a novel PET tracer based on a therapeutical drug candidate. VU6010572 exhibits potent binding affinity (IC $_{50}$ = 39.9 nM) and exceptional selectivity (>100-fold over other mGluR subtypes). Radiolabeling with fluorine-18 yielded [18 F]VU6010572 with high radiochemical yield (48%, decay-corrected) and molar activity (59 GBq/µmol). While *in vitro* autoradiography demonstrated heterogeneous brain distribution, dynamic PET imaging in rodents revealed reasonable brain uptake *in vivo* yet modest binding specificity and rapid brain washout. While these findings support the potential of [18 F]VU6010572 as a lead structure, further medicinal chemistry optimization is warranted to enhance the metabolic and pharmacokinetic properties.

Keywords: Metabotropic glutamate receptor 3, mGluR3, negative allosteric modulator, fluorine-18, positron emission tomography

Introduction

Glutamate is one of the primary excitatory neurotransmitters in the central nervous system and plays a critical role in regulating synaptic plasticity, learning, memory, and overall neural development and communication under physiological conditions [1, 2]. Glutamate exerts its effects through two major classes of receptors: ionotropic glutamate receptors (iGluRs), which are ligand-gated ion channels, and metabotropic glutamate receptors (mGluRs), which are G protein-coupled receptors (GPCRs). Based on sequence homology, pharmacological profiles, and signaling mechanisms, mGluRs are further subdivided into three groups (I-III) [3]. Among these, group II mGluRs - comprising mGluR2 and mGluR3 - are negatively coupled to adenylyl cyclase and function to suppress excitatory synaptic transmission through the inhibition of cyclic adenosine monophosphate (cAMP) production. In particular, mGluR3 is widely expressed in both neurons and glial cells, where it orchestrates complex intercellular signaling involved in neuroprotection, synaptic plasticity, and neuroinflammation. Its modulation of neuron-glia communication has been implicated in maintaining central nervous system homeostasis, particularly under conditions of stress or injury. mGluR3 dysfunction has been associated with several neuropsychiatric and neurodegenerative conditions, including schizophrenia, major depressive disorder, autism spectrum disorder, and Alzheimer's disease [4, 5]. These findings emphasize the relevance of mGluR3 as a therapeutic target.

Positron emission tomography (PET) is a powerful, noninvasive imaging modality that enables real-time monitoring of molecular and cellular processes *in vivo* with high sensitivity [6-8]. The development of PET radioligands targeting key neuroreceptors has reshaped our ability to assess disease pathophysiology, as well as pharmacodynamic responses, and guide the development of central nervous system therapeutics. Despite the biological relevance of mGluR3, efforts to develop selective PET tracers for this receptor subtype have yielded limited success. To date, only three mGluR3-targeted PET radioligands, [11C]CMG, [11C]CMGDE, and [11C]mG3N001 have been reported, yet most of them exhibit dual affinity for mGluR2 and mGluR3,



A Previous metabotropic glutamate receptor 3 PET tracers (not mGluR3 selective)

$$H_2N$$
 $O^{11}CH_3$ H_3CO $O^{11}CH_3$ H_2N $O^{11}CH_3$ H_2N $O^{11}CH_3$ $O^{11}CH_3$

B This work (mGluR3 selective)

[¹⁸F]VU6010572

limiting their utility for subtype-specific imaging (**Figure 1**) [9, 10]. To address this unmet need, we report on the radiolabeling and *in vivo* evaluation of [¹⁸F]VU6010572, a novel ¹⁸F-labeled PET radioligand with high affinity and high selectivity for mGluR3. Indeed, VU6010572 was identified through structure-activity relationship (SAR) optimization and demonstrated >100-fold selectivity over other mGluR subtypes. VU6010572 was successfully radiolabeled with fluorine-18 and subsequently evaluated in a series of preclinical studies, including *in vitro* autoradiography, dynamic PET imaging, whole-body biodistribution, and radiometabolite analysis in rodents. These efforts represent an important step toward enabling subtype-selective mGluR3-targeted imaging to support translational drug development.

Material and methods

General information

Chemicals were used directly in synthesis as purchased. The NMR data was recorded on a 300 or 400 MHz NMR spectrometer (see NMR spectra in <u>Supplementary Materials</u>). High-resolution mass (HRMS) data and low-resolution mass (liquid chromatography-mass spectrom-

Figure 1. Representative mGluR3 PET tracers. A. Previously reported mGluR3 PET tracers; B. [18F]VU6010572.

etry, LC-MS) data were recorded in APCI mode and ESI mode, respectively. Rodents were fed in a light/dark (12 h/12 h) cycle. Animal studies were conducted according to the ethical guidelines of Emory University.

Chemistry

Synthesis of 4-(benzyloxy)-1-(4-fluorophenyl)pyridin-2(1H)-one (2): To a solution of compound 1 (1.8 g, 9.0 mmol, 1.0 eq.) in CH₂Cl₂ (45 mL), (4-fluorophenyl)boronic acid (2.5 g, 18.0 mmol, 2.0 eq.), pyridine (1.6 ml, 19.9 mmol, 2.2 eq.), and copper (II) acetate (1.8 g, 9.9 mmol, 1.1 eq.) were added. The mixture was stirred at room temperature for 48 hours. Then the reaction mixture was washed with saturated aqueous sodium bicarbonate solution and brine, dried over Na₂SO₄, concentrated, and purified by flash chromatography to afford 2 (white solid, 2.0 g, 75% yield). 1 H NMR (400 MHz, DMSO-d6) δ 7.57 (d, J = 7.6 Hz, 1H), 7.48-7.37 (m, 7H), 7.32 (t, J = 8.8 Hz, 2H), 6.11 (dd, J = 7.6, 2.8 Hz, 1H), 5.98 (d, J = 2.8 Hz, 1H), 5.14 (s, 2H). LCMS (ESI): calcd for C₁₈H₁₅FNO₂+ (M + H+): 296.1, found 296.1.

Synthesis of 4-(benzyloxy)-1-(4-bromophenyl)pyridin-2(1H)-one (3): Compound 3 was prepared through the same pro-

cedure described for 2, except that (4-bromophenyl) boronic acid was used instead of (4-fluorophenyl)boronic acid. Compound 3 was obtained in 68% yield (white solid, 1.2 g). 1 H NMR (400 MHz, DMSO-d6) δ 7.68 (d, J = 8.4 Hz, 2H), 7.58 (d, J = 8.0 Hz, 1H), 7.47-7.33 (m, 7H), 6.12 (dd, J = 7.6, 2.8 Hz, 1H), 5.98 (d, J = 2.8 Hz, 1H), 5.14 (s, 2H). LCMS (ESI): calcd for $C_{18}H_{15}BrNO_2^+$ (M + H $^+$): 356.0, found 356.0.

Synthesis of 1-(4-fluorophenyl)-4-hydroxypyridin-2(1H)-one (4): To a solution of 2 (1.1 g, 3.7 mmol, 1.0 eq.) in MeOH (25 mL), Pd/C (240.0 mg, 10%) was added. The mixture was stirred at room temperature for 18 hours under the $\rm H_2$ atmosphere. The mixture was filtered and concentrated to afford 4 (yellow solid, 0.7 g, 92% yield), which was used directly in the next step.

Synthesis of 1-(4-bromophenyl)-4-hydroxypyridin-2(1H)-one (5): To a solution of 3 (1.42 g, 4.0 mmol, 1.0 eq.) in CH₂Cl₂ (120 mL), BBr₃ (3.0 g, 12.0 mmol, 3.0 eq.) was added at -10°C. The mixture was stirred at -10°C for 15 mins. Then the reaction was quenched with ice water and extracted with ethyl acetate. The organic layer was washed with water and brine, dried over Na₂SO₄, concentrated, and purified by flash chromatography to afford 5 (white solid, 0.8 g, 75% yield). ¹H NMR (400 MHz, DMSO-d6) δ 10.83 (s, 1H), 7.66 (dt, J = 9.6, 2.8 Hz, 2H), 7.51 (d, J = 7.6 Hz, 1H), 7.32 (dt, J = 8.8, 2.8 Hz, 2H), 5.97 (dd, J = 7.6, 2.4 Hz, 1H), 5.65 (d, J = 2.4 Hz, 1H). LCMS (ESI): calcd for C₁₁H₉BrNO₂+ (M + H+): 266.0, found 266.0.

Synthesis of (S)-1-(4-fluorophenyl)-4-(2-phenoxypropoxy) pyridin-2(1H)-one (6 or VU6010572): To a solution of 4 (205 mg, 1.0 mmol, 1.0 eq.) in THF (20 mL), (S)-2phenoxypropan-1-ol (182 mg, 1.2 mmol, 1.2 eq.), PPh₃ (576 mg, 2.2 mmol, 2.2 eq.), DtBAD (di-tert-butyl azodicarboxylate, 368 mg, 1.6 mmol, 1.6 eq.) were added at 0°C. The reaction was stirred at room temperature for 12 h. Then the mixture was concentrated and purified by flash chromatography to afford 6 or VU6010572 (220 mg, 65% yield) as a white solid. ¹H NMR (400 MHz, Chloroform-d) δ 7.34-7.28 (m, 4H), 7.19-7.13 (m, 3H), 7.00-6.95 (m, 3H), 6.01 (dd, J = 7.6, 2.8 Hz, 1H), 5.97 (d, J = 2.8 Hz, 1H), 4.76 (m, 1H), 4.14 (dd, J = 10.0, 6.0 Hz, 1H), 4.04 (dd, J = 10.4, 4.4 Hz, 1H), 1.43 (d, J = 6.4 Hz, 3H). ¹³C NMR (100 MHz, Chloroform-d) δ 167.5, 163.8, 162.1 (d, J = 229.1), 157.5, 137.7, 136.5 (d, J = 3.3 Hz), 129.6, 128.5 (d, J = 8.7 Hz), 121.5, 116.3 (d, J = 22.8 Hz), 116.2, 101.7, 98.2, 71.8, 71.1, 16.8. LCMS (ESI): calcd for $C_{20}H_{10}FNO_3^+$ (M + H⁺): 340.1, found 340.1.

Synthesis of (S)-1-(4-bromophenyl)-4-(2-phenoxypropoxy) pyridin-2(1H)-one (7): Through the same procedure as 6, compound 7 was obtained (white solid, 0.8 g, 87% yield). 1 HNMR (400 MHz, DMSO-d6) δ 7.68 (d, J = 8.8 Hz, 2H), 7.55 (d, J = 7.6 Hz, 1H), 7.34 (d, J = 8.4 Hz, 2H), 7.29 (dd, J = 8.8, 7.6 Hz, 2H), 6.99 (d, J = 7.6 Hz, 2H), 6.94 (t, J = 7.6 Hz, 1H), 6.06 (dd, J = 7.6, 2.4 Hz, 1H), 5.93 (d, J = 2.8 Hz,

1H), 4.83 (m, 1H), 4.17 (m, 2H), 1.32 (d, J = 6.4 Hz, 3H). LCMS (ESI): calcd for $\rm C_{20}H_{19}BrNO_3^+$ (M + H $^+$): 400.1, found 400.1.

Synthesis of (S)-4-(2-phenoxypropoxy)-1-(4-(4,4,5,5-tetramethyl-1,3,2-dioxaborolan-2-yl)phenyl)pyridin-2(1H)one (8): To a solution of 7 (0.8 g, 2.0 mmol, 1.0 eq.) in 1,4-dioxane (110 mL), B₂Pin₂ (1.27 g, 5.0 mmol, 2.5 eq.), KOAc (588 mg, 6.0 mmol, 3.0 eq.), and Pd(dppf)Cl₂ (220 mg, 0.3 mmol, 0.15 eq.) were added. The mixture was stirred at 80°C for 12 hours under the N₂ atmosphere. The mixture was concentrated and purified by flash chromatography to afford 8 (200 mg, 22% yield) as a white solid. 1 HNMR (400 MHz, Chloroform-d) δ 7.91 (d, J = 8.0 Hz, 2H), 7.36 (d, J = 8.4 Hz, 2H), 7.30 (dd, J = 8.8, 7.6 Hz, 2H), 7.20 (d, J = 7.6 Hz, 1H), 6.99 (d, J = 7.2, 1H), 6.96 (d, J = 7.6, 2H), 6.00 (dd, J = 7.6, 2.8 Hz, 1H), 5.96 (d, J = 2.4Hz, 1H), 4.76 (m, 1H), 4.14 (dd, J = 10.0, 6.0 Hz, 1H), 4.04(dd, J = 10.0, 4.0 Hz, 1H), 1.43 (d, J = 6.0 Hz, 3H), 1.35 (s, J = 612H). ¹³C NMR (75 MHz, Chloroform-d) δ 167.3, 163.6, 157.5, 143.0, 137.6, 135.8, 129.6, 125.8, 121.4, 116.2, 101.4, 98.2, 84, 71.8, 71.0, 24.8, 16.8 Hz. HRMS (APCI): for $C_{26}H_{31}BNO_{5}$ (M + H⁺): 448.2290, found 448.2294.

Pharmacology

The mGlu3 human glutamate (metabotropic) GPCR cell-based cAMP leadhunter assay with compound VU6010572 was performed by Eurofins. VU6010572 was tested in negative allosteric modulator mode.

Radiochemistry

An aliquot of [¹⁸F]fluoride was added to a vial with tetraethylammonium bicarbonate (TEAB, 1 mg) and dried with nitrogen gas flow at 110°C. When the vial was dry, acetonitrile (1 mL) was added, and the drying process was repeated. Then precursor 8 (2 mg) and [Cu(Py)₄(OTf)₂] (7 mg) in DMAc/nBuOH (0.2/0.1 mL) were added and heated at 110°C under the air atmosphere for 20 min. After that, the reaction mixture was diluted with water and passed through Sep-Pak light C18, which was eluted with MeCN and diluted with water for HPLC purification (see HPLC radio-chromatograms in Supplementary Materials).

In vitro stability

According to a previous report [11], [18F]VU6010572 was incubated with saline, serums of mouse, rat, NHP, and human at 37°C. At 5, 30, 60, or 120 minutes after incubation with [18F]VU6010572, the samples were mixed with cold MeCN and centrifuged, and the supernatants were analyzed by radio-HPLC.

In vitro autoradiography

According to a previous report [12], the rat brain sections were incubated with Tris-HCl buffer (50 mM) and then [18F]VU6010572 at room temperature. For the blocking study, incubation was conducted with VU6010572 (10

Figure 2. Synthesis of VU6010572 (6) and its labeling precursor 8. Reaction conditions: (i) (4-fluorophenyl)boronic acid (for 2) or (4-bromophenyl)boronic acid (for 3), pyridine, $Cu(OAc)_2$, CH_2Cl_2 , N_2 , RT, 48 h, 60% yield for 2 and 65% yield for 3; (ii) Pd/C, H_2 , MeOH, r.t., 18 h, 95% yield; (iii) Pd/C, P

 μ M) and [18 F]VU6010572. After that, the brain sections were washed with cold Tris-HCl buffer (2 minutes) and distilled water (10 seconds). Then the dried brain sections were positioned on an imaging screen and scanned by the Typhoon biomolecular imager.

PET imaging

As previously reported [13, 14], PET imaging of [18F] VU6010572 (0.04 mCi) in CD-1 mice was performed in a Genisys G8 PET scanner for 1 hour. Mice were pre-treated with VU6010572 (3 mg/kg, i.v.) 10 minutes before administration of [18F]VU6010572 in the blocking study.

Whole-body biodistribution

According to the previous reports [7, 15], CD-1 mice were administered with [18 F]VU6010572 (10 μ Ci) and then euthanized at 5, 15, 30, and 60 minutes, respectively. Major organs were weighed and measured by a gamma counter.

Radiometabolite analysis

Radiometabolite analysis of [18F]VU6010572 was conducted according to a previous report [16]. CD-1 mice were administered with [18F]VU6010572 and then euthanized 30 minutes after administration of [18F] VU6010572. The brain samples were homogenized and centrifuged with cold MeCN and PBS buffer. After that, the supernatants were analyzed by radio-HPLC. The col-

lected [18F]VU6010572 and its 18F-metabolites were measured by a gamma counter. The plasma samples were analyzed through the same procedure described for the brain samples.

Results

Chemistry

The synthesis of compound VU6010572 commenced with a copper-mediated cross-coupling reaction of 4-(benzyloxy)pyridin-2(1*H*)-one 1 and (4-fluorophenyl)boronic acid, generating compound 2 in 60% yield (Figure 2). After the deprotection of the benzyl group in the presence of Pd/C and hydrogen gas, intermediate 3 was obtained in 95% yield. Finally, the condensation reaction of compound 3 and (S)-2-phenoxypropan-1-ol afforded VU6010572 in 65% yield. In short, VU6010572 was synthesized in 37% overall yield over three steps. Similar to the synthesis of VU6010572, its borate precursor was prepared from the cross-coupling reaction of compound 1 and (4-bromophenyl)boronic acid, deprotection of the benzyl group, condensation reaction with (S)-2-phenoxypropan-1-ol, and the following Pd-catalyzed boration reaction. Finally, the borate precursor 8 was obtained in 12% overall yield over four steps.

Pharmacology

The mGlu3 human glutamate (metabotropic) GPCR cell-based cAMP leadhunter assay was performed with com-

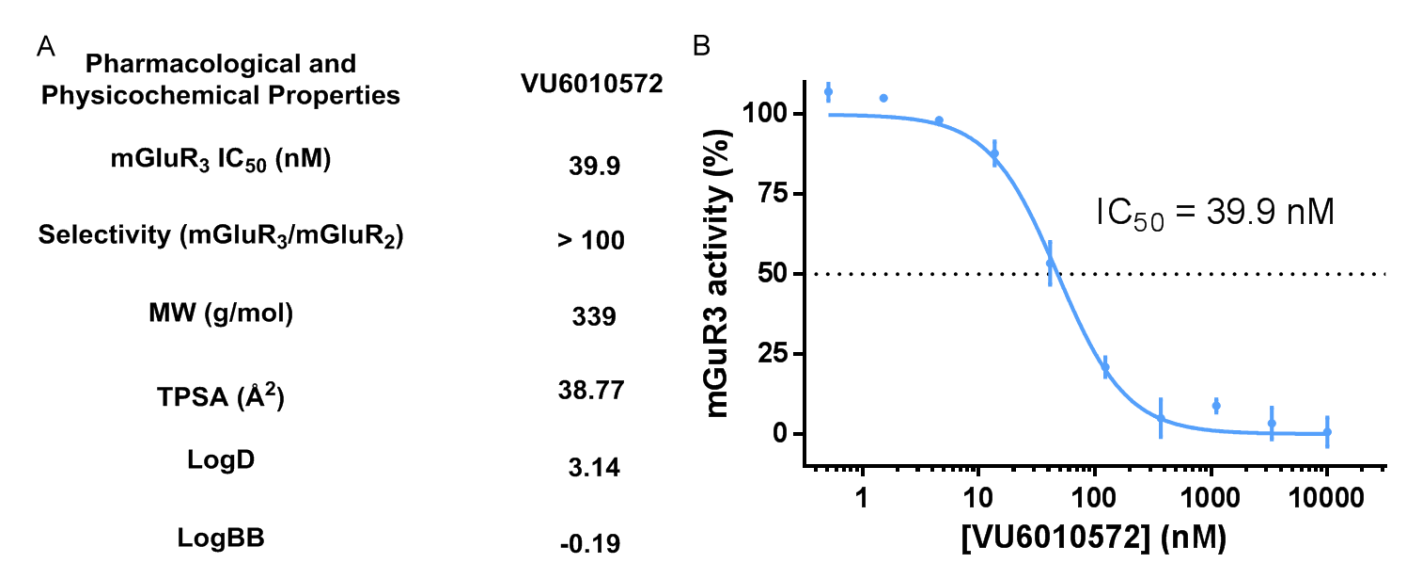


Figure 3. Pharmacological profile of VU6010572. A. Representative pharmacological and physicochemical properties of VU6010572; B. Concentration-response curve of VU6010572 for inhibiting mGluR3 activity.

pound VU6010572 in negative allosteric modulator mode and VU6010572 showed an IC $_{50}$ value of 39.9 nM (**Figure 3**). VU6010572 had more than 100-fold mGluR3 selectivity over all other mGluRs [17]. Its topological polar surface area (tPSA = 38.77) was predicted by ChemDraw and the logD (3.14) was measured by the shake flask method [18]. The blood-brain barrier (BBB) permeability for VU6010572 (logBB = -0.19) was predicted by ACD/Percepta. Furthermore, an off-target binding screen was conducted for VU6010572 (<u>Figure S1</u>), and no significant off-target binding (>50% inhibition) was observed against 61 major central nervous system (CNS) targets.

Radiochemistry and in vitro stability

As shown in **Figure 4A**, VU6010572 was labeled with fluorine-18 through Cu-mediated $^{18}\text{F-fluorination}$ of precursor 8 using [^{18}F]Et $_{_4}\text{NF}$ in DMAc/tBuOH at 110°C for 20 minutes [19]. [^{18}F]VU6010572 was obtained in 48% decay-corrected radiochemical yield with molar activity of 59 GBq/µmol (1.6 Ci/µmol). The *in vitro* stability of [^{18}F] VU6010572 was tested in saline and serum across different species. No decomposition was detected in saline for up to 120 minutes (**Figure 4B**). Furthermore, the stability of [^{18}F]VU6010572 in the serum of rodents, NHP, and human revealed minimal radiometabolite presence for up to 60 minutes with incubation at 37°C (**Figure 4C-F**).

In vitro autoradiography

To assess the regional binding distribution and specificity of [18F]VU6010572, *in vitro* autoradiography was performed using rat brain sections. As illustrated in **Figure 5**, [18F]VU6010572 exhibited heterogeneous binding across brain regions, with prominent accumulation observed in the cortex, thalamus, and striatum, regions known to express high levels of mGluR3, and lower levels of radio-

tracer uptake detected in the cerebellum and pons, consistent with the relatively sparse expression of mGluR3 in these areas [20]. To confirm target-specific binding, competition studies were performed by co-incubating brain slices with an excess of non-radioactive VU6010572 (10 μ M). This resulted in a notable reduction in tracer binding within mGluR3-enriched regions, with signal intensity decreased by approximately 31-36% in the cortex, thalamus, and striatum. These findings support the conclusion that [18 F]VU6010572 binds selectively to mGluR3 *in vitro*, establishing a foundation for its further evaluation as a PET radioligand *in vivo*.

PET imaging

To evaluate the *in vivo* pharmacokinetic profile and brain penetration of [¹⁸F]VU6010572, dynamic microPET imaging was performed in CD-1 mice over a 60-minute scan duration. As shown in **Figure 6**, [¹⁸F]VU6010572 successfully crossed the blood-brain barrier, achieving an initial brain uptake of 2.5 SUV at 1-minute post-injection, followed by a fast brain clearance.

To investigate binding specificity *in vivo*, blocking studies were conducted using an intravenous pretreatment with non-radioactive VU6010572 (3 mg/kg). No substantial reduction in overall brain uptake was observed (Figure S2), suggesting a high proportion of nonspecific signal or rapidly reversible binding. However, when blood radioactivity was accounted for, a modest reduction in brain-associated signal was detected - specifically, a 13% decrease in PET signal at 45 minutes post-injection - supporting partial target engagement by the blocker (Figure S3). These results demonstrate that [18F]VU6010572 is brain-penetrant and serves as an initial scaffold for further optimization as an mGluR3-selective PET radioligand, albeit additional refinements may be required to improve *in vivo* binding specificity [21].

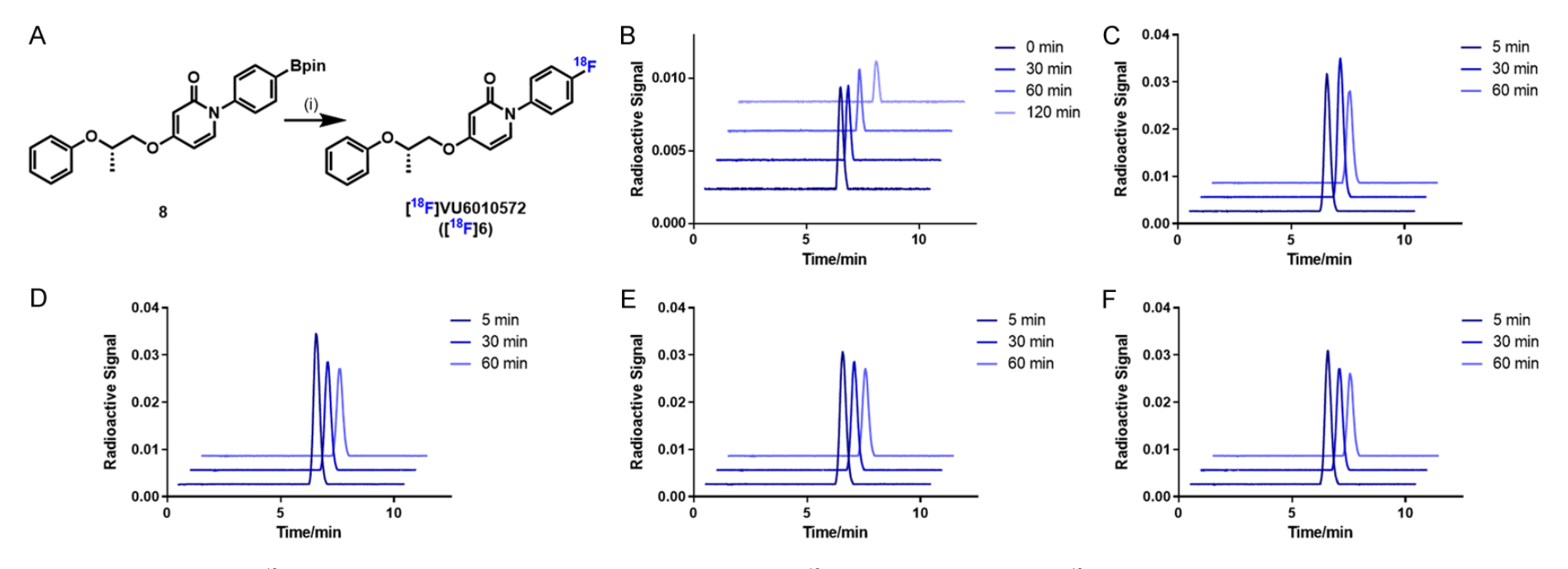


Figure 4. Radiosynthesis of [^{18}F]VU6010572 and in vitro stability tests. A. Radiosynthesis of [^{18}F]VU6010572, conditions (i) [^{18}F]Et $_4$ NF, [Cu(Py) $_4$ (OTf) $_2$], DMAc/nBuOH, 110 °C, 20 min, 48% RCY (decay-corrected); B. Stability of [^{18}F]VU6010572 in mouse serum; D. Stability of [^{18}F]VU6010572 in rat serum; E. Stability of [^{18}F]VU6010572 in NHP serum; F. Stability of [^{18}F]VU6010572 in human serum.

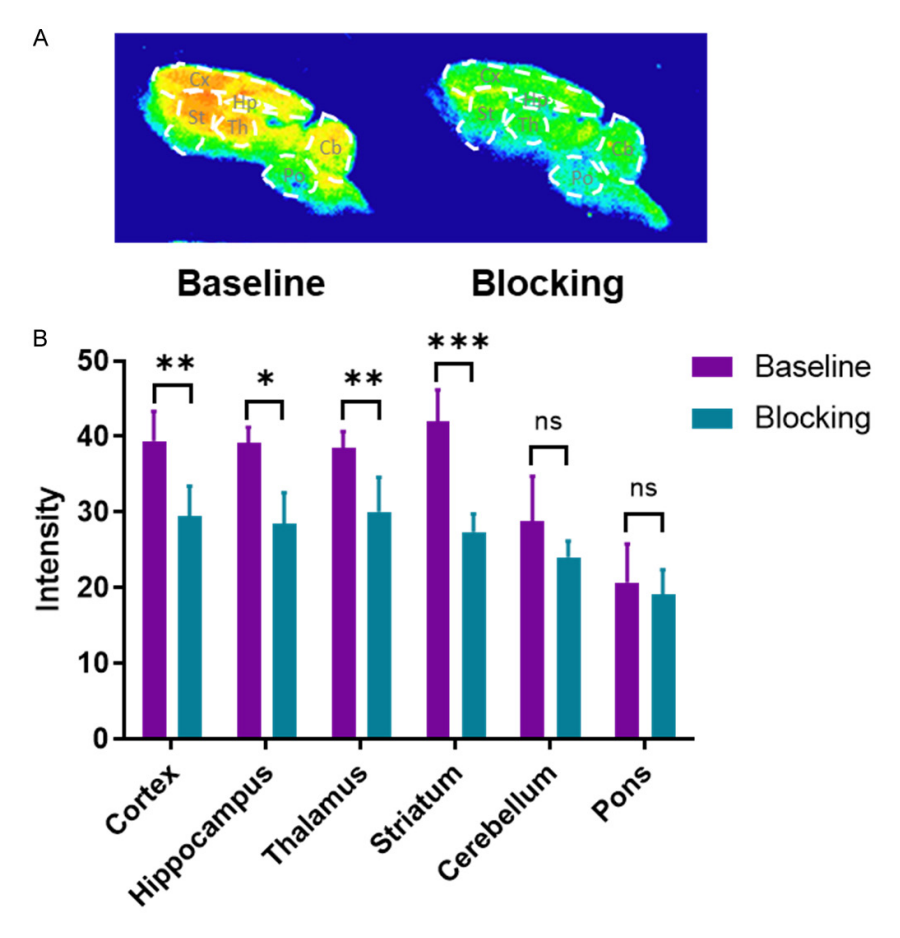


Figure 5. Autoradiography of [18 F]VU6010572 in rat brains. A. Representative images for baseline and blocking autoradiography studies with [18 F]VU6010572; B. Quantification of autoradiography studies with [18 F]VU6010572. Cx, cortex; Hp, hippocampus; Th, thalamus; St, striatum; Cb, cerebellum; Po, pons. All data are mean \pm SD, n = 5.

Whole-body biodistribution

To characterize the peripheral distribution and clearance profile of [18F]VU6010572, whole-body biodistribution studies were performed in CD-1 mice at multiple time points following intravenous injection. As shown in Figure 7 and Table S1, the tracer exhibited initially high uptake (>5 %ID/g) in several organs, including the heart, lungs, pancreas, liver, small intestine, and kidneys - reflecting perfusion-related delivery and tissue-specific retention, respectively. Over the course of 60 minutes, a general decline in radioactivity levels was observed across most tissues. Notably, the small intestine and liver exhibited sustained uptake, with levels remaining elevated at 14.8 %ID/g and 5.6 %ID/g, respectively, at 60-minute post-injection. These findings suggest a hepatobiliary route of excretion, likely contributing to the prolonged retention in gastrointestinal tissues. Importantly, no appreciable accumulation of radioactivity was observed in the bone throughout the study duration, indicating limited in vivo defluorination.

Radiometabolite analysis

The metabolic stability of [18F]VU6010572 was assessed in CD-1 mice via ex vivo radiometabolite analysis of plas-

ma and brain samples collected 30 minutes post-injection (Figure 8). In the brain, only 63% of the radioactivity corresponded to the intact parent compound, indicating a substantial fraction of radiolabeled metabolites within the CNS. In plasma, 38% of the radioactivity is attributable to [18F]VU6010572 at 30 min post-injection. For brain PET tracers, it is generally envisioned that the vast majority of the brain signal arises from the unchanged parent compound, as the presence of brain-penetrant radiometabolites can confound quantitative analysis and complicate interpretation of regional binding. The detection of significant metabolite-derived signal in the brain suggests that [18F]VU6010572 undergoes metabolic degradation with generation of radiometabolites capable of crossing the blood-brain barrier. In general, the presence of radiometabolites in peripheral compartments such as plasma can be addressed by correcting it using the arterial input function. Overall, the radiometabolite data raises important limitations regarding the suitability of [18F] VU6010572 for quantitative brain imaging, which emphasizes the need for further structural optimization to enhance metabolic stability and reduce the formation of brain-penetrant radiometabolites.

Discussion

To date, only three ¹¹C-labeled PET radioligand have been reported for imaging mGluR3, yet most of them exhibit similar binding affinities toward mGluR2 and mGluR3, precluding selective imaging of the mGluR3 subtype. In an effort to address this gap, we explored [18F] VU6010572, a novel ligand with excellent in vitro selectivity for mGluR3 (>100-fold over all other mGluRs) [17]. In the human mGluR3 cAMP-based assay, VU6010572 demonstrated favorable potency and in silico prediction was projected the compound to be brain-penetrant. The compound also exhibited no off-target activity across a panel of 61 CNS targets, confirming its high selectivity in the brain. VU6010572 was efficiently labeled with fluorine-18 using a copper-mediated approach, yielding [18F] VU6010572 with high radiochemical yield (48%, decaycorrected) and molar activity (59 GBq/µmol). The radiotracer displayed excellent in vitro stability in saline and serum from mouse, rat, non-human primate, and human sources, indicating its suitability for preclinical imaging studies. In vitro autoradiography using rat brain sections confirmed regionally specific accumulation of [18F]

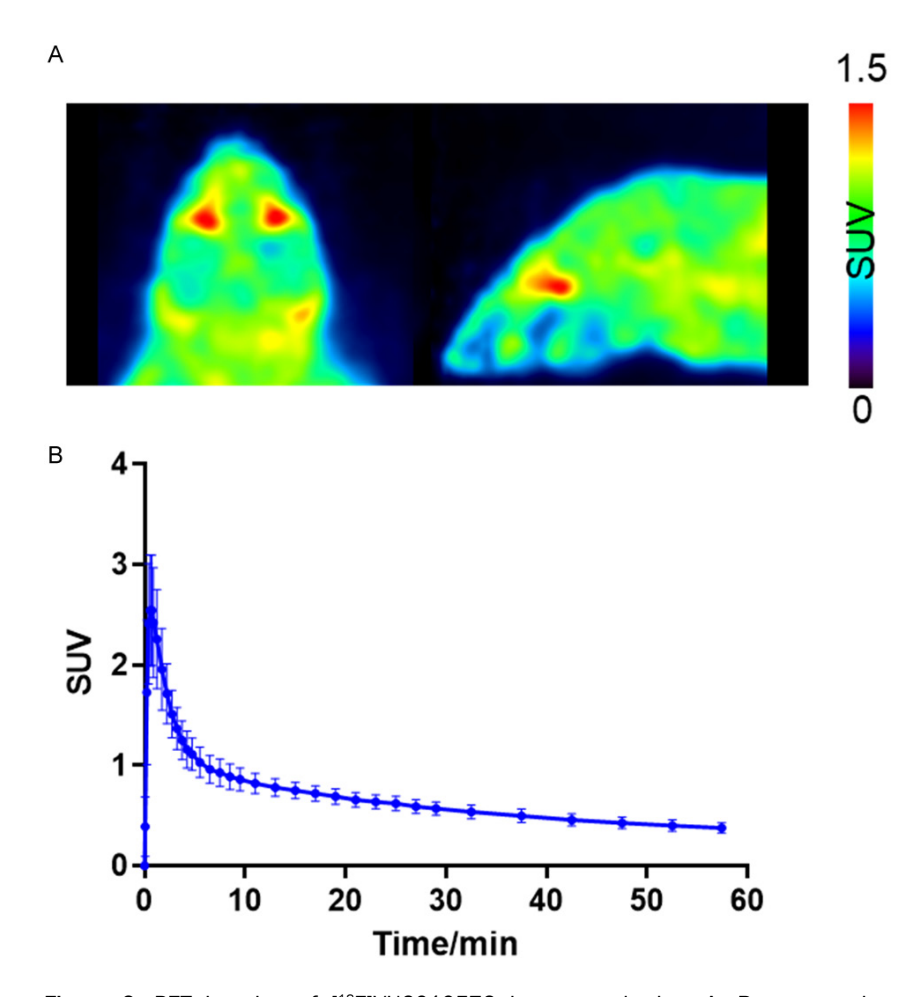


Figure 6. PET imaging of [18 F]VU6010572 in mouse brains. A. Representative summed PET images (0-60 minutes) of [18 F]VU6010572 in mouse brains; B. Time-activity curve of [18 F]VU6010572 in the whole brain. All data are mean \pm SD, n = 4.

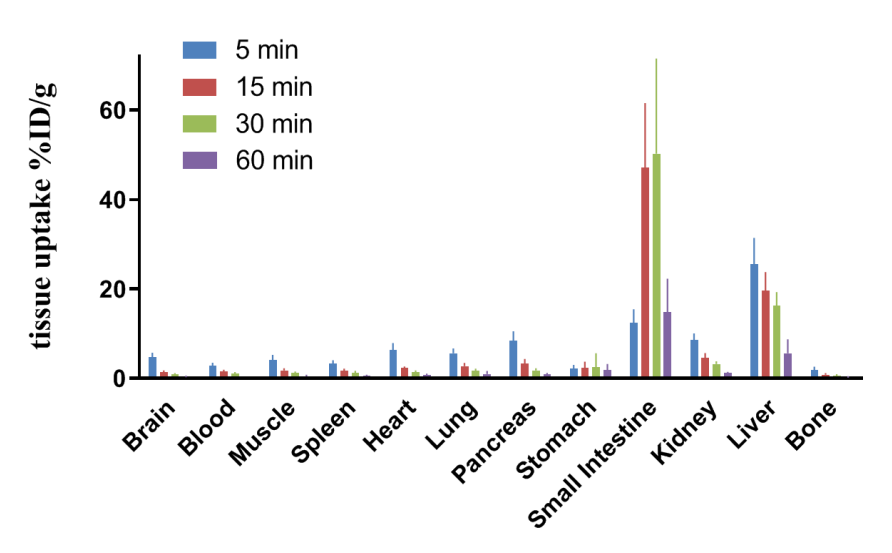


Figure 7. Whole-body biodistribution study of [18 F]VU6010572 in CD-1 mice. All data are mean \pm SD, n = 3.

VU6010572 in mGluR3-enriched regions, including the cortex, thalamus, and striatum, with lower uptake in the hippocampus, cerebellum, and pons [20]. Importantly, pretreatment with non-radioactive VU6010572 substan-

tially reduced signal intensity in these high-expression areas, indicating high binding specificity under *in vitro* conditions.

In vivo PET imaging in CD-1 mice demonstrated that [18F]VU6010572 crossed the blood-brain barrier and exhibited reasonable brain uptake (SUV of ca. 2.5 at 1 min), followed by rapid washout. Pretreatment with the unlabeled ligand did not lead to a marked reduction in total brain uptake, suggesting limited target-specific binding in vivo. Notably, when blood radioactivity was accounted for, a modest 13% reduction in brain signal at 45 minutes post-injection was observed [21], which may be attributed to the blocking of mGluR3, leading to an increased concentration of free [18F] VU6010572 in circulation. The wholebody biodistribution profile revealed high early uptake in organs such as the small intestine, liver, and kidneys, consistent with a combination of hepatobiliary and renal elimination. The absence of bone uptake throughout the imaging period suggests metabolic stability of the radiolabel, with negligible in vivo defluorination.

Despite promising in vitro results, radiometabolite analysis revealed that only 63% of radioactivity in the brain corresponded to intact [18F]VU6010572 at 30 minutes post-injection. Indeed, the presence of a substantial fraction of brainassociated radiometabolites in this study indicates that metabolic degradation of [18F]VU6010572 generates radiolabeled species capable of crossing the bloodbrain barrier - thereby limiting its suitability for quantitative PET imaging. Taken together, [18F]VU6010572 represents a starting point for the development of selective mGluR3 PET tracers, with favorable in vitro binding characteristics, blood-brain barrier permeability, and metabolic stability against defluorination. However, the partial metabolic instability in vivo, particularly with radiometabolites in the brain, highlights the need for further medicinal chemistry efforts to

enhance metabolic resistance and eliminate confounding radiometabolite signals. Such refinements will be critical to realizing the full translational potential of mGluR3-targeted PET imaging.

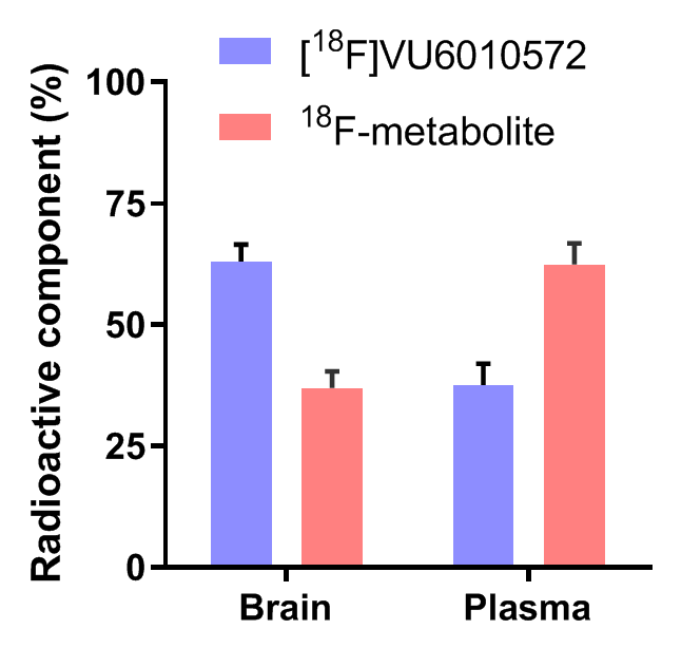


Figure 8. Radiometabolite analysis of [18 F]VU6010572 in CD-1 mice. All data are mean \pm SD, n = 3.

Conclusion

VU6010572 was identified as a potent and selective negative allosteric modulator of mGluR3 and was successfully radiolabeled with fluorine-18, yielding a PET tracer with high radiochemical efficiency and molar activity. While in vitro autoradiography displayed regionally heterogeneous brain uptake consistent with mGluR3 expression, and exhibited specific binding in mGluR3-enriched regions, in vivo PET imaging confirmed that [18F] VU6010572 crossed the blood-brain barrier with limited binding specificity. The presence of brain-penetrant radiometabolites and low specific signal present limitations for its use in quantitative in vivo imaging. Continued medicinal chemistry optimization will be required to explore structure-activity relationships (SAR) and modify the phenoxy group, aiming to design novel candidates with enhanced metabolic stability and improved pharmacokinetic properties for the development of a suitable mGluR3 PET radioligand.

Acknowledgements

We thank Emory Center for Systems Imaging Radio-pharmacy (Ronald J. Crowe, RPh, BCNP; Karen Dolph, RPh; M. Shane Waldrep) & Department of Radiology and Imaging Sciences, Emory University School of Medicine for general support. We also thank the National Institute of Mental Health's Psychoactive Drug Screening Program (NIMH PDSP) for compound off-target screening. J.S.P. is supported by NCI T32CA275777. H.Y. is supported by NIH/NICHD (HD082373). S.H.L. gratefully acknowledges the support provided, in part, by the NIH grants (MH117125 and NS130128), Emory Radiology Chair

Fund, and Emory School of Medicine Endowed Directorship. We thank Emory Center for Systems Imaging for assistance with small animal micro-PET/CT system, which was funded by NIH grant (S100D034326) and Emory Integrated Core Facilities.

Disclosure of conflict of interest

None.

Address correspondence to: Steven H Liang, Department of Radiology and Imaging Sciences, Emory University, Atlanta, Georgia 30322, The United States. E-mail: steven.liang@emory.

References

- [1] Zhou Y and Danbolt NC. Glutamate as a neurotransmitter in the healthy brain. J Neural Transm (Vienna) 2014; 121: 799-817.
- [2] Hansen KB, Wollmuth LP, Bowie D, Furukawa H, Menniti FS, Sobolevsky AI, Swanson GT, Swanger SA, Greger IH, Nakagawa T, McBain CJ, Jayaraman V, Low CM, Dell'Acqua ML, Diamond JS, Camp CR, Perszyk RE, Yuan H and Traynelis SF. Structure, function, and pharmacology of glutamate receptor ion channels. Pharmacol Rev 2021; 73: 298-487.
- [3] Reiner A and Levitz J. Glutamatergic signaling in the central nervous system: ionotropic and metabotropic receptors in concert. Neuron 2018; 98: 1080-1098.
- [4] Ribeiro FM, Vieira LB, Pires RG, Olmo RP and Ferguson SS. Metabotropic glutamate receptors and neurodegenerative diseases. Pharmacol Res 2017; 115: 179-191.
- [5] Dogra S and Conn PJ. Metabotropic glutamate receptors as emerging targets for the treatment of schizophrenia. Mol Pharmacol 2022; 101: 275-285.
- [6] Deng X, Rong J, Wang L, Vasdev N, Zhang L, Josephson L and Liang SH. Chemistry for positron emission tomography: recent advances in ¹¹C-, ¹⁸F-, ¹³N-, and ¹⁵O-labeling reactions. Angew Chem Int Ed Engl 2019; 58: 2580-2605.
- [7] Rong J, Zhao C, Xia X, Li G, Haider A, Wei H, Chen J, Xiao Z, Li Y, Zhou X, Xu H, Collier TL, Wang L and Liang SH. Evaluation of [18F]Favipiravir in rodents and Nonhuman Primates (NHP) with positron emission tomography. Pharmaceuticals (Basel) 2023; 16: 524.
- [8] Rong J and Liu Y. Advances in medical imaging techniques. BMC Methods 2024; 1: 10.
- [9] Wang JQ, Zhang Z, Kuruppu D and Brownell AL. Radiosynthesis of PET radiotracer as a prodrug for imaging group II metabotropic glutamate receptors in vivo. Bioorg Med Chem Lett 2012; 22: 1958-1962.
- [10] Wang J, Wang C, El Fakhri G, Caravan P, Zhang Z and Brownell AL. Development of [11C]mG3N001 as a PET imaging ligand for metabotropic glutamate receptor 3 (mGluR3). J Nucl Med 2020; 61: 1041.
- [11] Rong J, Zhao C, Chaudhary AF, Jones E, Van R, Song Z, Li Y, Chen J, Zhou X, Patel JS, Gao Y, Sun Z, Feng S, Zhang Z, Collier TL, Ran C, Haider A, Shao Y, Yuan H and Liang SH. Development of a novel ¹⁸F-labeled radioligand for imaging phosphodiesterase 7 with positron emission tomography. Mol Pharm 2025; 22: 1657-1666.

- [12] Rong J, Yamasaki T, Li Y, Kumata K, Zhao C, Haider A, Chen J, Xiao Z, Fujinaga M, Hu K, Mori W, Zhang Y, Xie L, Zhou X, Collier TL, Zhang MR and Liang S. Development of novel ¹¹C-labeled selective orexin-2 receptor radioligands for positron emission tomography imaging. ACS Med Chem Lett 2023; 14: 1419-1426.
- [13] Rong J, Mori W, Xia X, Schafroth MA, Zhao C, Van RS, Yamasaki T, Chen J, Xiao Z, Haider A, Ogasawara D, Hiraishi A, Shao T, Zhang Y, Chen Z, Pang F, Hu K, Xie L, Fujinaga M, Kumata K, Gou Y, Fang Y, Gu S, Wei H, Bao L, Xu H, Collier TL, Shao Y, Carson RE, Cravatt BF, Wang L, Zhang MR and Liang SH. Novel reversible-binding PET ligands for imaging monoacylglycerol lipase based on the piperazinyl azetidine scaffold. J Med Chem 2021; 64: 14283-14298.
- [14] Shao T, Chen Z, Rong J, Belov V, Chen J, Jeyarajan A, Deng X, Fu H, Yu Q, Rwema SH, Lin W, Papisov M, Josephson L, Chung RT and Liang SH. [18F]MAGL-4-11 positron emission tomography molecular imaging of monoacylglycerol lipase changes in preclinical liver fibrosis models. Acta Pharm Sin B 2022; 12: 308-315.
- [15] Rong J, Zhao C, Chaudhary AF, Chen J, Zhou X, Zhang K, Song Z, Sun Z, Gao Y, Zhang Z, Feng S, Collier TL, Yuan H, Patel JS, Haider A, Li Y and Liang SH. Development of a novel ¹⁸F-labeled radioligand for imaging cholesterol 24-hydroxylase with positron emission tomography. ACS Pharmacol Transl Sci 2025; 8: 800-807.
- [16] Rong J, Yamasaki T, Chen J, Kumata K, Zhao C, Fujinaga M, Hu K, Mori W, Zhang Y, Xie L, Chaudhary AF, Zhou X, Zhang W, Gao Y, Zhang K, Patel JS, Song Z, Collier TL, Yuan H, Ran C, Haider A, Li Y, Zhang MR and Liang S. Development of a candidate ¹¹C-labeled selective phosphodiesterase 1 radioligand for positron emission tomography. ACS Omega 2024; 9: 44154-44163.

- [17] Engers JL, Bollinger KA, Weiner RL, Rodriguez AL, Long MF, Breiner MM, Chang S, Bollinger SR, Bubser M, Jones CK, Morrison RD, Bridges TM, Blobaum AL, Niswender CM, Conn PJ, Emmitte KA and Lindsley CW. Design and synthesis of *N*-Aryl phenoxyethoxy pyridinones as highly selective and CNS penetrant mGlu₃ NAMs. ACS Med Chem Lett 2017; 8: 925-930.
- [18] OECD. Test No. 107: partition coefficient (n-octanol/water): Shake Flask Method. 1995.
- [19] Tredwell M, Preshlock SM, Taylor NJ, Gruber S, Huiban M, Passchier J, Mercier J, Génicot C and Gouverneur V. A general copper-mediated nucleophilic ¹⁸F fluorination of arenes. Angew Chem Int Ed Engl 2014; 53: 7751-7755.
- [20] Ohishi H, Shigemoto R, Nakanishi S and Mizuno N. Distribution of the mRNA for a metabotropic glutamate receptor (mGluR3) in the rat brain: an in situ hybridization study. J Comp Neurol 1993; 335: 252-266.
- [21] Horti AG, Naik R, Foss CA, Minn I, Misheneva V, Du Y, Wang Y, Mathews WB, Wu Y, Hall A, LaCourse C, Ahn HH, Nam H, Lesniak WG, Valentine H, Pletnikova O, Troncoso JC, Smith MD, Calabresi PA, Savonenko AV, Dannals RF, Pletnikov MV and Pomper MG. PET imaging of microglia by targeting macrophage colony-stimulating factor 1 receptor (CSF1R). Proc Natl Acad Sci U S A 2019; 116: 1686-1691.

Supplementary Materials

HPLC radio-chromatograms of [18F]VU6010572

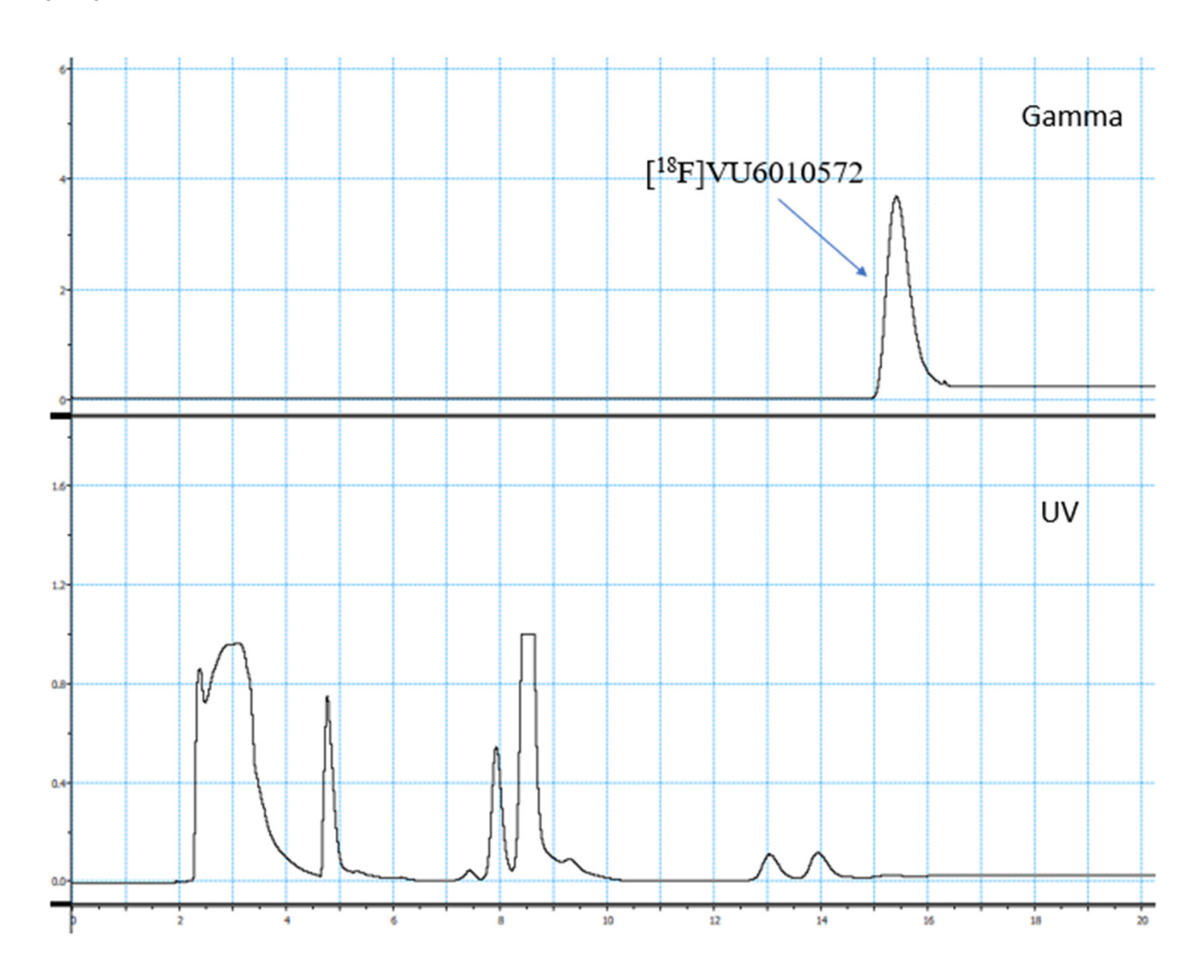
Semi-prep radio-HPLC chromatogram of [18F]VU6010572

Column: Phenomenex Luna® 5 μ m C18(2) 100 Å Prep Column (10 × 250 mm)

Mobile phase: $CH_3CN-H_2O = 45\%-55\%$ (containing 0.1% TFA)

flow rate: 5.0 mL/min

UV: 254 nm



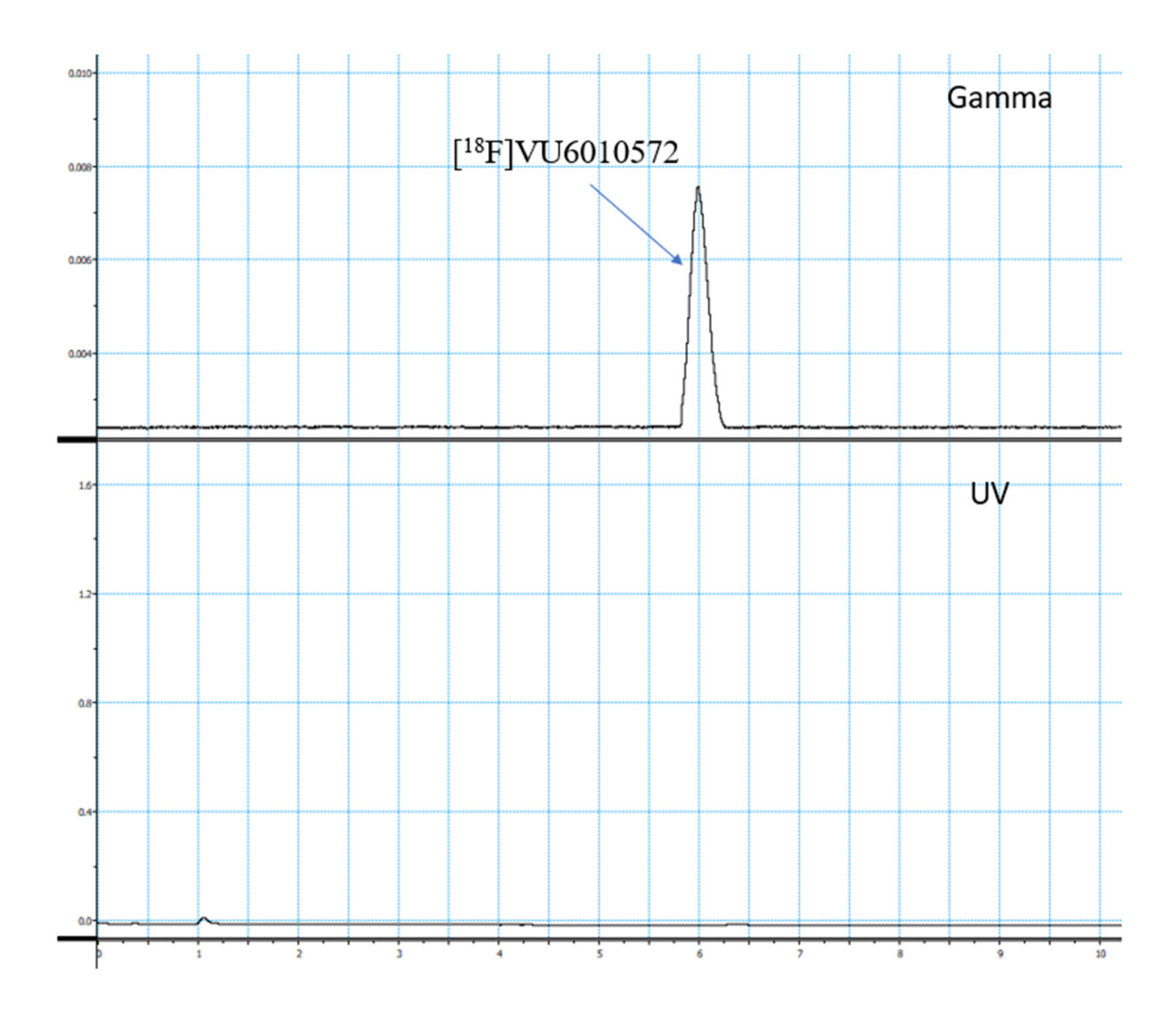
Analytical radio-HPLC chromatogram of [18F]VU6010572

Column: XBridge C18 3.5 μ m column (4.6 \times 100 mm)

Mobile phase: $CH_3CN-H_2O = 45\%-55\%$ (containing 0.1% TFA)

flow rate: 1.0 mL/min

UV: 254 nm



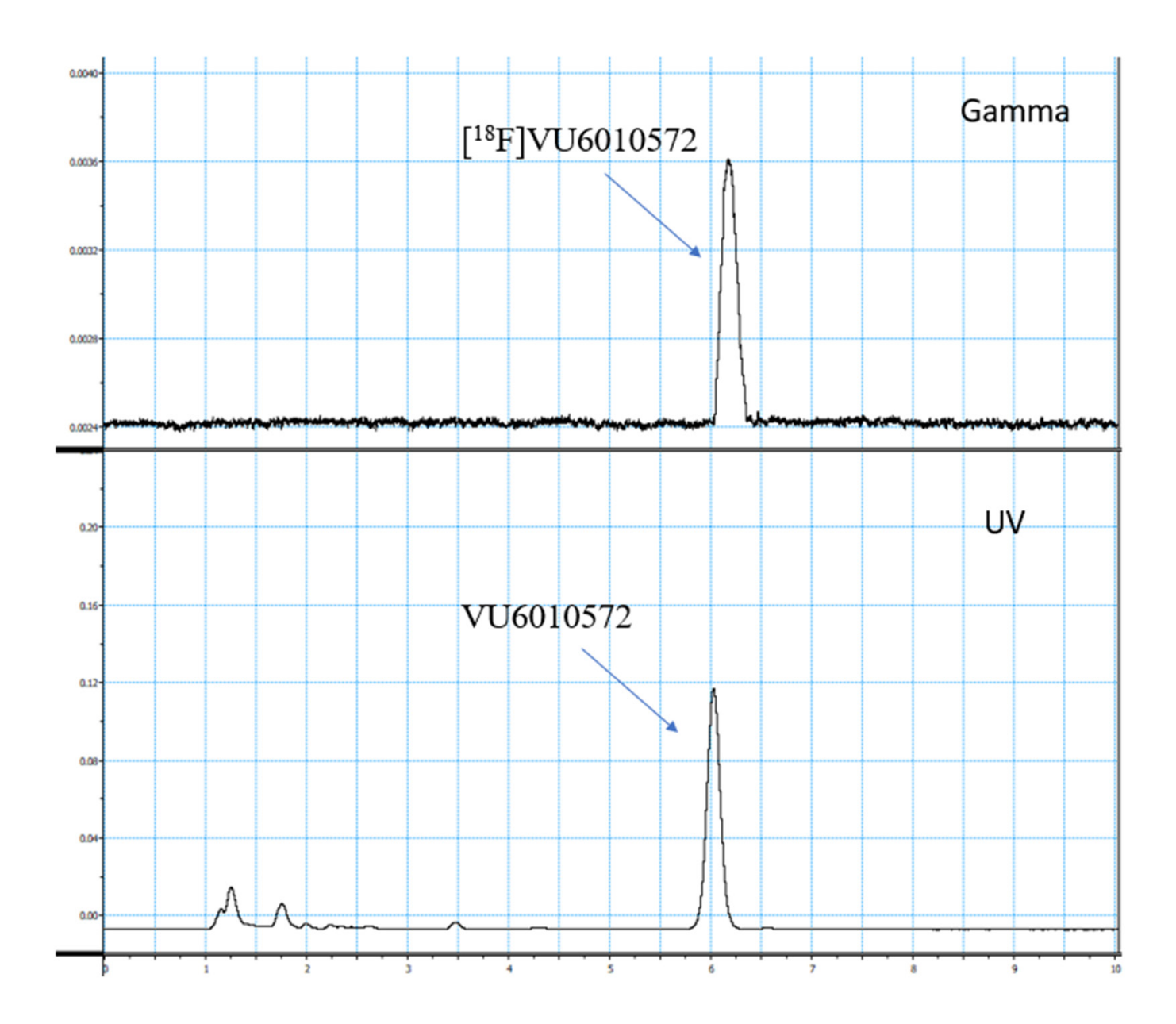
Co-injection of [18F]VU6010572 with unlabeled VU6010572

Column: XBridge C18 3.5 μ m column (4.6 \times 100 mm)

Mobile phase: $CH_3CN-H_2O = 45\%-55\%$ (containing 0.1% TFA)

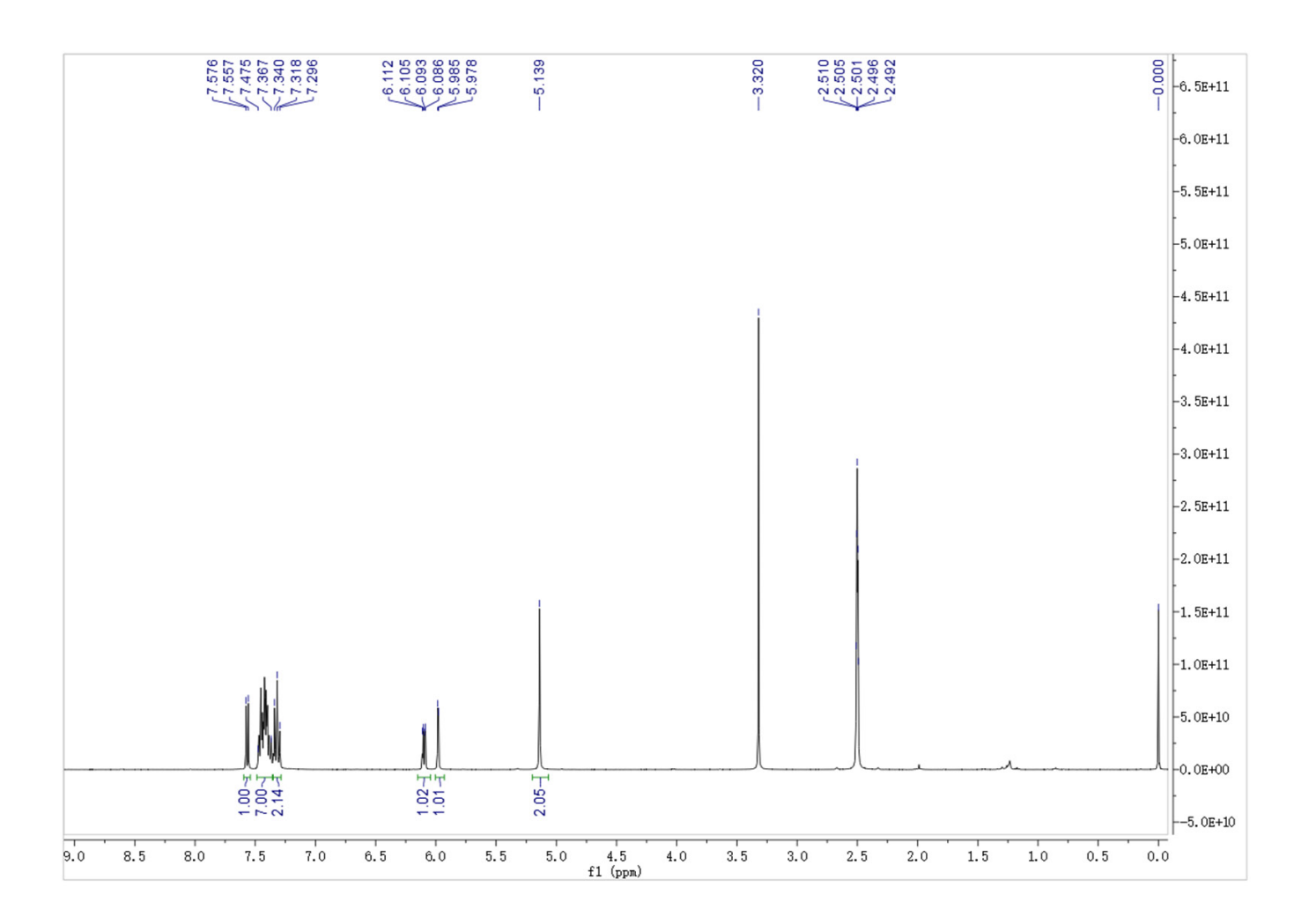
flow rate: 1.0 mL/min

UV: 254 nm

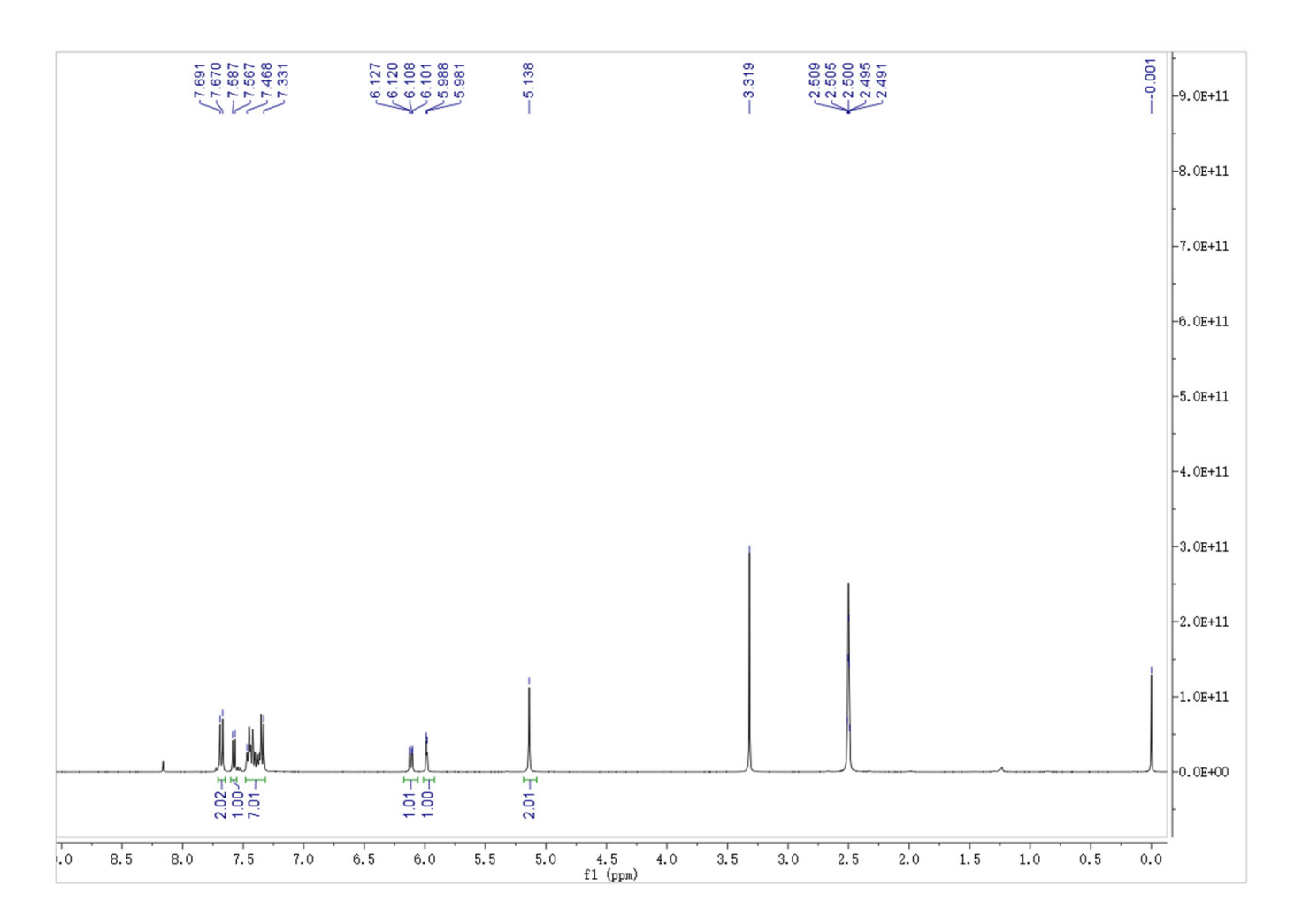


NMR spectra of isolated compounds

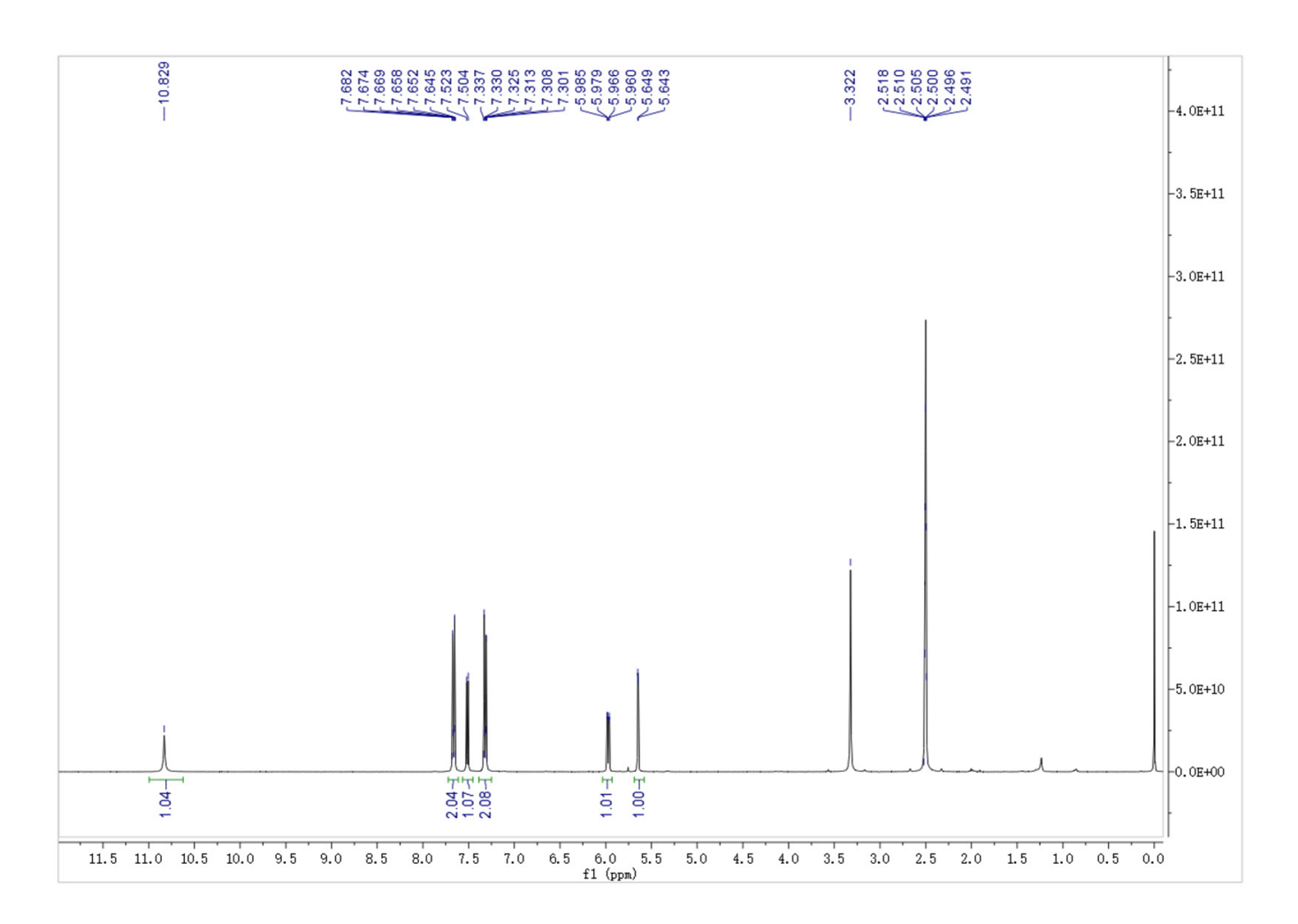
¹H NMR spectra of compound 2 (DMSO-d6, 400 MHz)



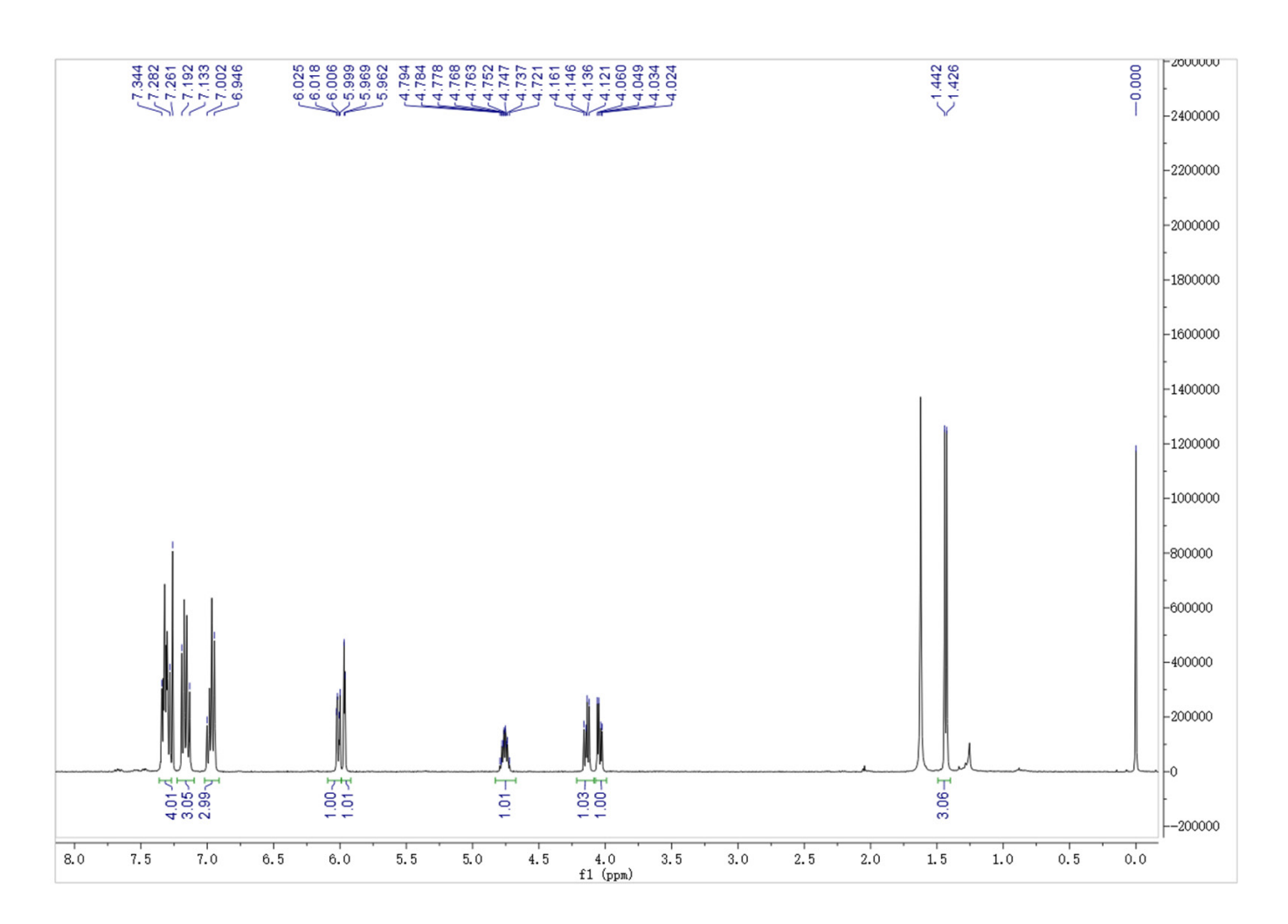
¹H NMR spectra of compound 3 (DMSO-d6, 400 MHz)



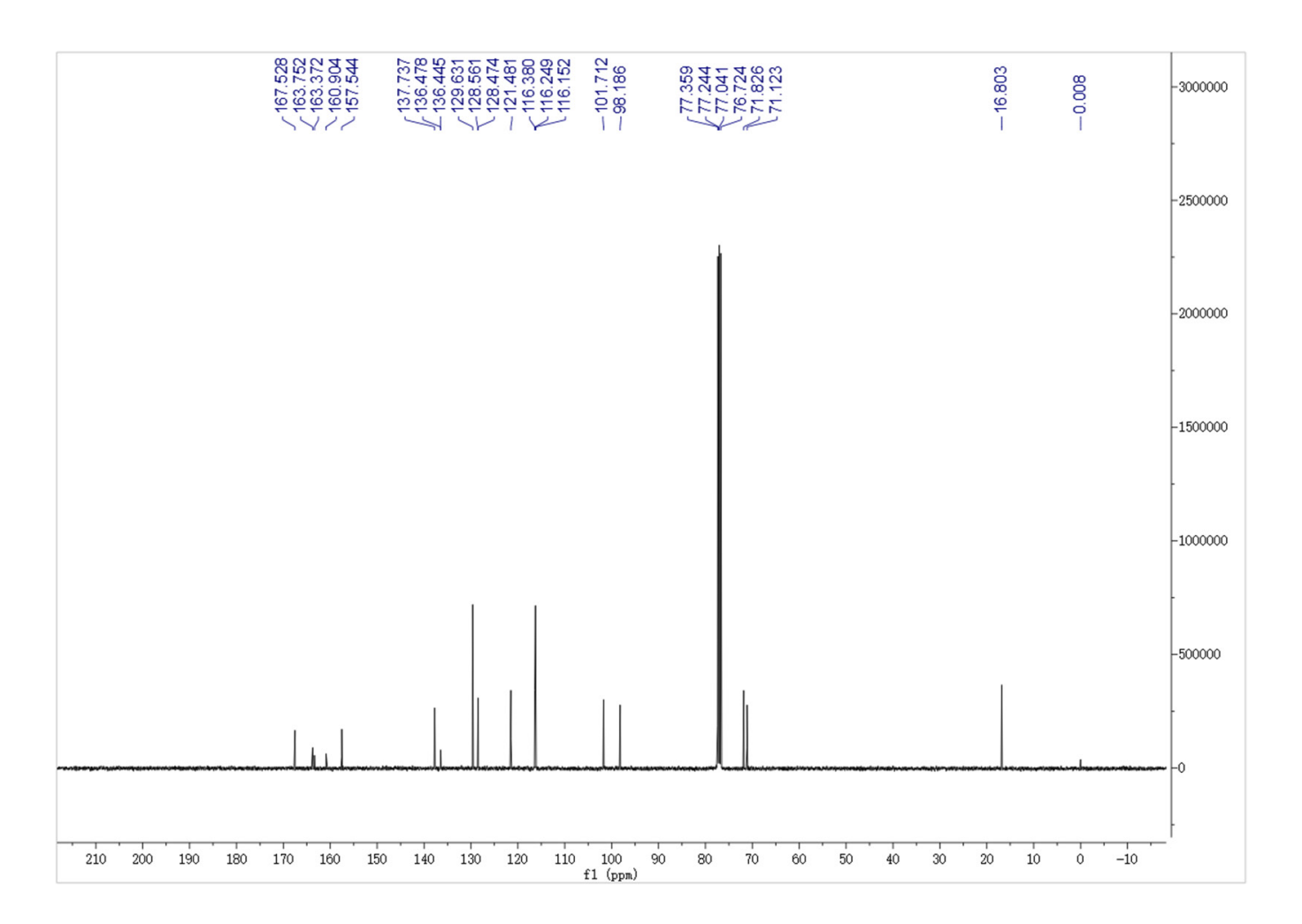
¹H NMR spectra of compound 5 (DMSO-d6, 400 MHz)



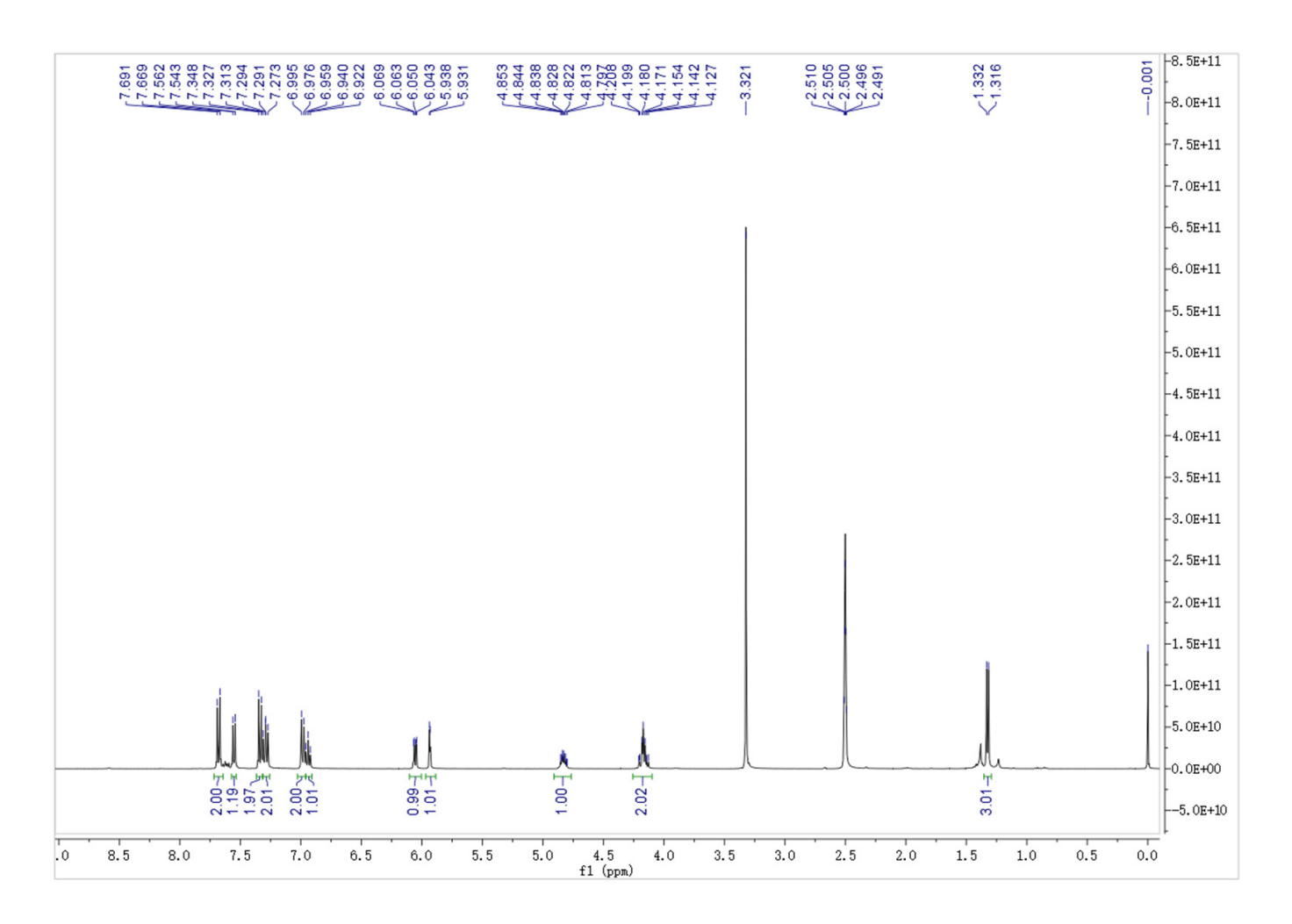
¹H NMR spectra of compound 6 (Chloroform-d, 400 MHz)



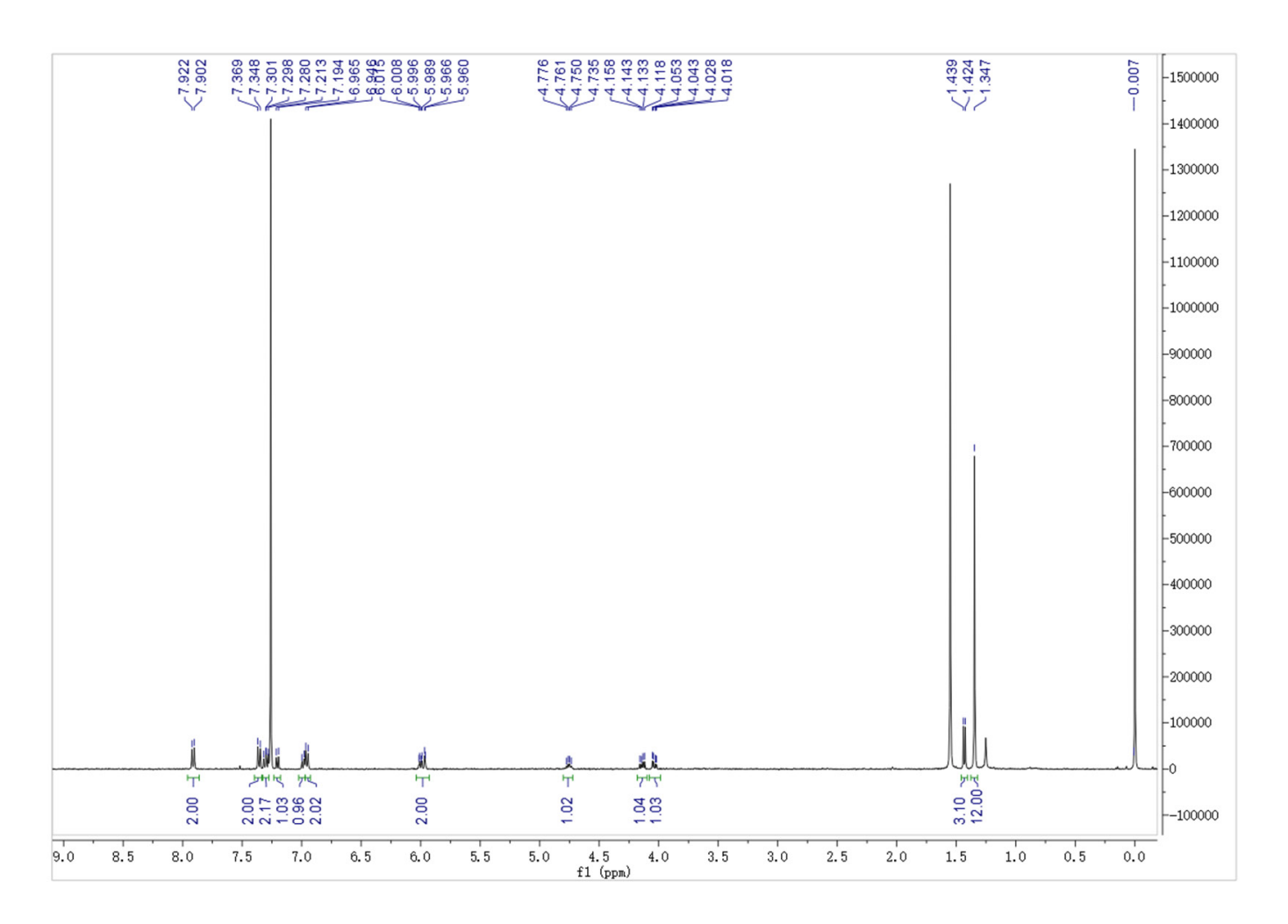
¹³C NMR spectra of compound 6 (Chloroform-d, 100 MHz)



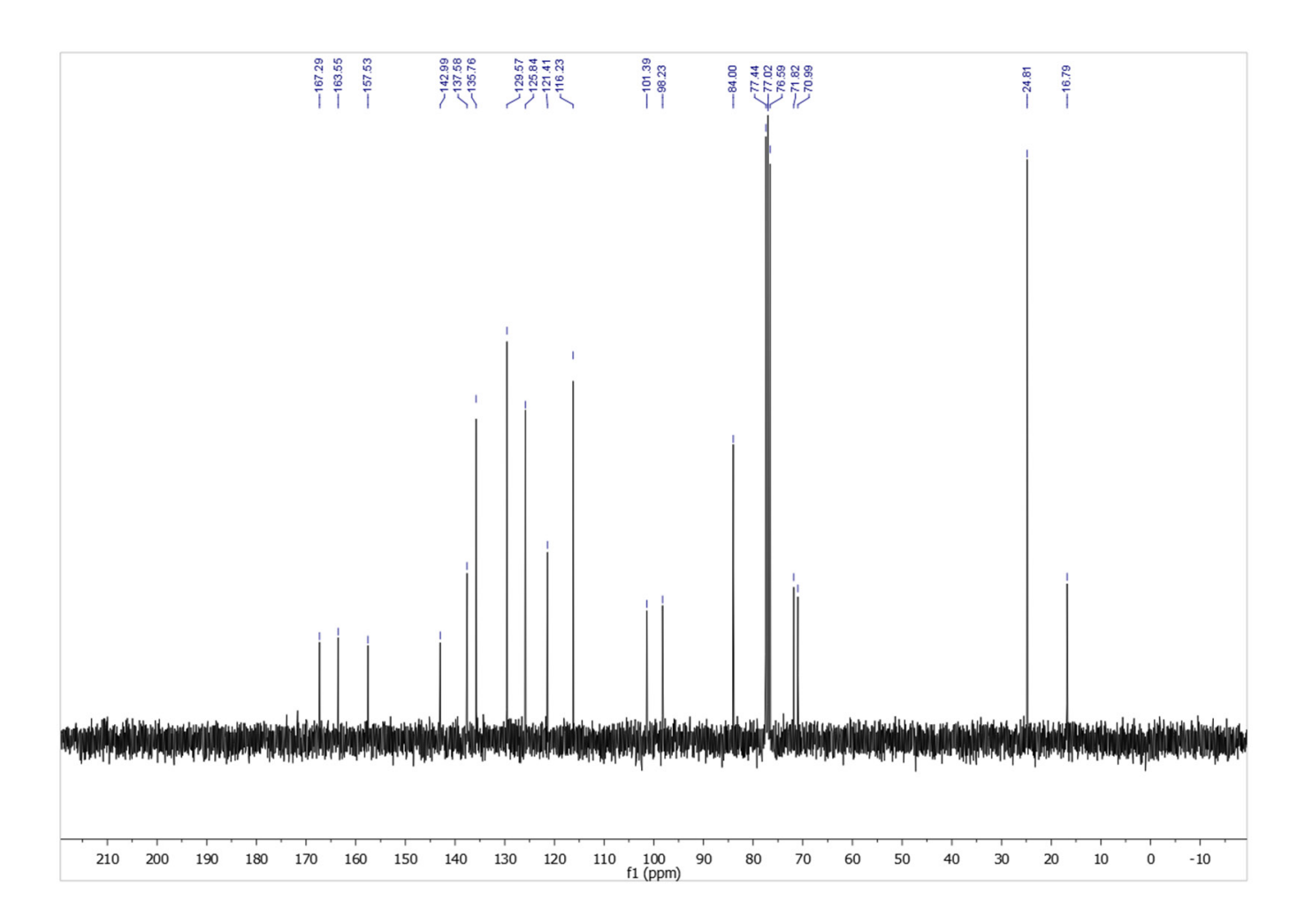
¹H NMR spectra of compound 7 (DMSO-d6, 400 MHz)



¹H NMR spectra of compound 8 (Chloroform-d, 400 MHz)



¹³C NMR spectra of compound 8 (Chloroform-d, 75 MHz)



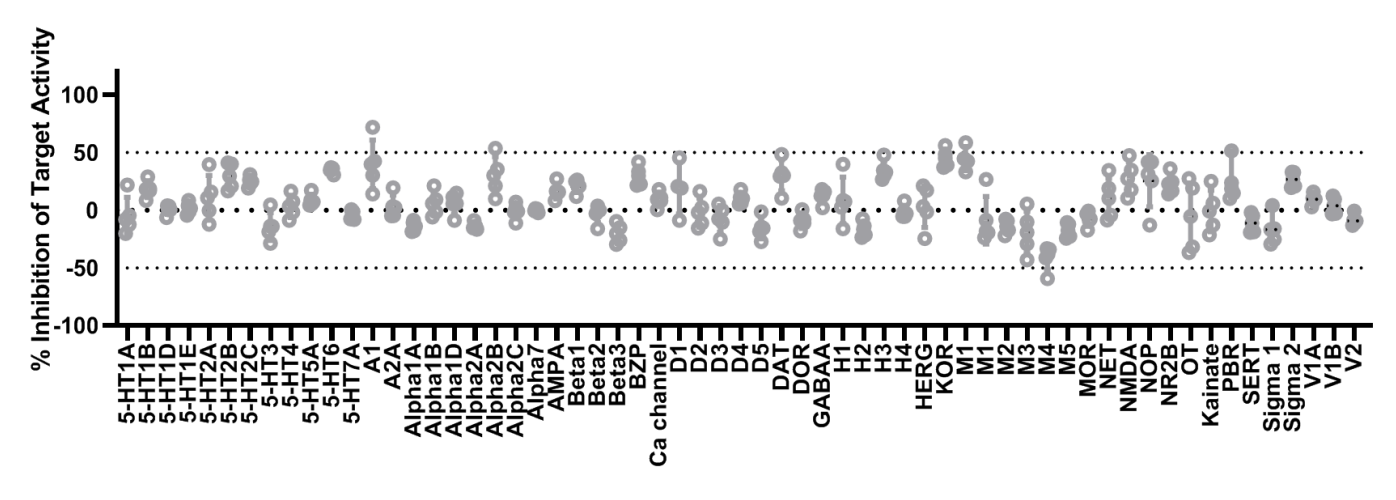


Figure S1. Off-target pharmacological evaluation of compound VU6010572 against 61 major CNS targets, including common GPCRs, enzymes, ion channels, and transporters: initial screening at a concentration of 10 μ M (supported by the NIMH PDSP). All data are mean \pm SD (n \geq 4). No significant off-target binding (>50%) was observed at 10 μ M compound testing concentration.

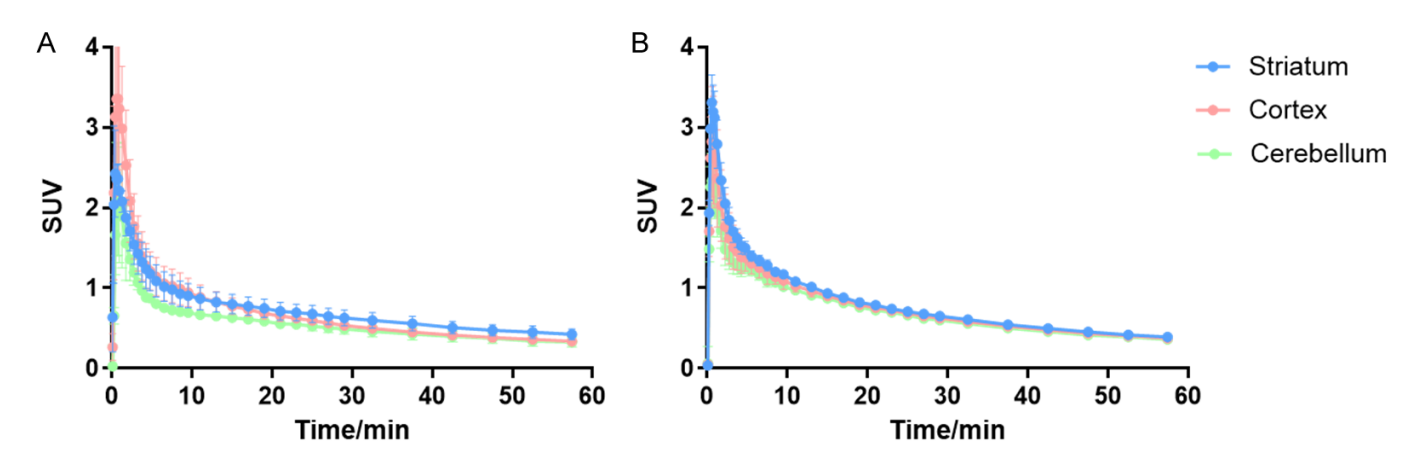


Figure S2. Time-activity curves of [18 F]VU6010572 in the mouse brain regions of interest in baseline (A) and bocking (B, VU6010572, 3 mg/kg) conditions ($n \ge 3$).

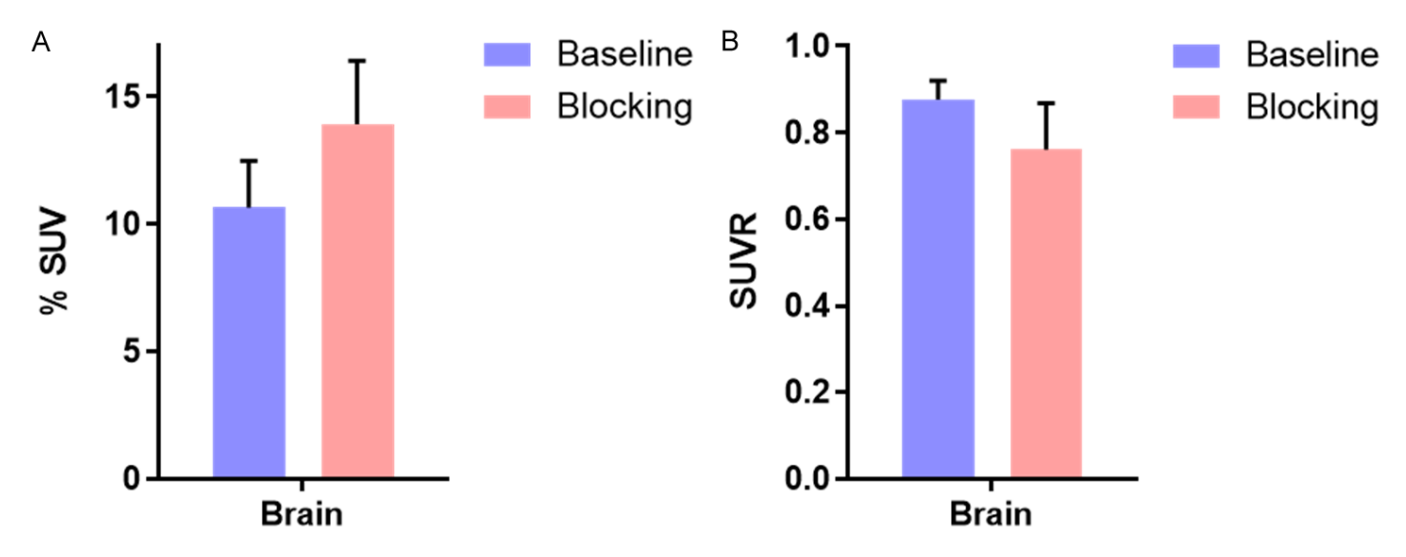


Figure S3. Brain uptake of [18 F]VU6010572 in CD-1 mouse brains at 45 min after radiotracer injection without (A) and with (B) blood correction. All data are mean \pm SD, n = 3.

Table S1. Whole-body ex vivo biodistribution study of [18 F]VU6010572 in CD-1 mice

ID%/g	5 min			15 min			30 min			60 min		
	Mean	SD	N	Mean	SD	N	Mean	SD	N	Mean	SD	N
Brain	4.69	0.86	3	1.45	0.16	3	0.89	0.07	3	0.42	0.02	3
Blood	2.85	0.47	3	1.53	0.26	3	1.11	0.12	3	0.52	0.02	3
Muscle	4.06	0.99	3	1.76	0.31	3	1.22	0.11	3	0.51	0.10	3
Spleen	3.33	0.52	3	1.62	0.36	3	1.19	0.34	3	0.55	0.07	3
Heart	6.34	1.40	3	2.29	0.22	3	1.40	0.17	3	0.66	0.21	3
Lung	5.59	0.92	3	2.74	0.55	3	1.73	0.27	3	1.02	0.45	3
Pancreas	8.43	1.93	3	3.31	0.84	3	1.79	0.27	3	0.88	0.19	3
Stomach	2.10	0.72	3	2.34	1.20	3	1.88	2.92	3	1.87	1.19	3
Small Intestine	12.39	2.88	3	47.14	14.30	3	50.25	21.10	3	14.79	7.30	3
Kidney	8.60	1.28	3	4.56	0.95	3	3.24	0.42	3	1.18	0.08	3
Liver	25.53	5.71	3	19.62	4.00	3	16.26	2.87	3	5.60	2.96	3
Bone	1.90	0.55	3	0.60	0.19	3	0.58	0.17	3	0.20	0.11	3

Data are mean \pm SD, n = 3.